

## Photochemical Reduction of Nitrate and Nitrite by Manganese and Iron Porphyrins

Kenneth S. Suslick\* and Randall A. Watson

Received October 12, 1990

New nitrate and nitrite complexes of metalloporphyrins have been synthesized and crystallographically characterized, and their photochemistry has been examined. Irradiation of  $\text{Mn}(\text{TPP})(\text{NO}_3)$  and  $\text{Mn}(\text{TPP})(\text{NO}_2)$  (where TPP = 5,10,15,20-tetra-phenylporphyrinate(2-)) produces the high-valent metal-oxo species  $\text{O}=\text{Mn}^{\text{IV}}(\text{TPP})$  quantitatively, with quantum yields of  $1.58 \times 10^{-4}$  and  $5.30 \times 10^{-4}$ , respectively. This metal-oxo species is capable of oxidizing substrates, as demonstrated in reactions with styrene or triphenylphosphine.  $\text{Mn}(\text{TPP})(\text{NO}_2)$  is formed as an intermediate in the complete photolysis of  $\text{Mn}(\text{TPP})(\text{NO}_3)$ . Similarly, the photochemistry of  $\text{Fe}(\text{TPP})(\text{NO}_3)$  produces substrate oxidation, including C-H hydroxylation, which suggests the photochemical formation of  $\text{O}=\text{Fe}^{\text{IV}}(\text{TPP}^{*+})$  as the active oxidant. Remarkably, all three oxygen atoms of the initially bound  $\text{NO}_3^-$  can be used for substrate oxidation. The X-ray crystal structures of  $\text{Mn}(\text{TPP})(\text{NO}_3) \cdot 2\text{C}_6\text{H}_6$  and  $\text{Mn}(\text{TPP})(\text{NO}_2) \cdot \text{C}_6\text{H}_6$  have been solved. In the nitrate complex  $\text{Mn}(\text{TPP})(\text{NO}_3)$ , the average Mn-pyrrole N distance is 2.007 Å, with the metal 0.21 Å above the mean plane of the nitrogen atoms. The nitrate ion is coordinated in a unidentate fashion with a Mn-O bond length of 2.101 Å.  $\text{Mn}(\text{TPP})(\text{NO}_2)$  is the first metalloporphyrin complex with oxygen-bound nitrite. The average Mn-pyrrole nitrogen distance is 2.012 Å, with the metal 0.23 Å above the mean plane of the nitrogen atoms. The nitrite ion is coordinated through one of the oxygens, with a Mn-O bond length of 2.059 Å. Crystal data for  $\text{Mn}(\text{TPP})(\text{NO}_3) \cdot 2\text{C}_6\text{H}_6$  at  $-76^\circ\text{C}$ : space group  $P\bar{1}$ ,  $a = 13.271$  (4) Å,  $b = 13.610$  (5) Å,  $c = 12.880$  (3) Å,  $\alpha = 111.44$  (2)°,  $\beta = 95.71$  (2)°,  $\gamma = 85.50$  (3)°,  $V = 2152$  (2) Å<sup>3</sup>,  $Z = 2$ ,  $R_F = 0.063$ ,  $R_{wF} = 0.086$  for 408 variables and 4890 unique data with  $I > 2.58\sigma(I)$ . Crystal data for  $\text{Mn}(\text{TPP})(\text{NO}_2) \cdot \text{C}_6\text{H}_6$ : space group  $Pccn$ ,  $a = 21.631$  (11) Å,  $b = 19.941$  (12) Å,  $c = 17.991$  (6) Å,  $V = 7760$  (7) Å<sup>3</sup>,  $Z = 8$ ,  $R_F = 0.062$ ,  $R_{wF} = 0.096$  for 543 variables and 3820 unique data with  $I > 2.58\sigma(I)$ .

## Introduction

Metalloporphyrins serve many functions in biological systems. Their important role in the reduction of oxoanions,<sup>1</sup> such as nitrite and sulfite in bacteria, and in the oxidation of organic substrates<sup>2</sup> by cytochrome P450, has prompted our current investigations into the photochemistry of metalloporphyrin complexes of nitrate and nitrite. We report here the novel photochemical reduction of  $\text{Mn}(\text{TPP})(\text{NO}_3)$  and  $\text{Mn}(\text{TPP})(\text{NO}_2)$  to produce  $\text{O}=\text{Mn}^{\text{IV}}(\text{TPP})$ , together with their synthesis and full characterization, including the single-crystal X-ray structures of  $\text{Mn}(\text{TPP})(\text{NO}_3)$  and  $\text{Mn}(\text{TPP})(\text{NO}_2)$ . We also report the photochemical transformation of  $\text{Fe}(\text{TPP})(\text{NO}_3)$  to  $[\text{Fe}(\text{TPP})]_2(\text{O})$  and present evidence for the intermediate formation of  $\text{O}=\text{Fe}^{\text{IV}}(\text{TPP}^{*+})$ . The unusual photochemical generation of metal-oxo species in all three systems can be used to produce oxidation of added substrates, often in quantitative yield.

Metal-free porphyrin photochemistry has been extensively scrutinized, especially for use in photodynamic cancer therapies.<sup>3</sup> Recently, the photochemistry of metalloporphyrins has garnered much interest.<sup>4-12</sup> Among metalloporphyrins, manganese and iron complexes have received the greatest attention. For iron, this is due in part to its direct relevance to numerous biological systems. Manganese porphyrins are of interest because of extensive mixing of the metal  $e_g$  orbitals and porphyrin ring  $e_g(\pi^*)$  orbitals.<sup>4</sup> This produces an intense charge-transfer band at relatively low energy (470-480 nm) and several transitions at higher energy, giving these complexes so-called "hyper" spectra. The mixing of excited states extends the possible types of photochemical reaction pathways. Though iron porphyrins occasionally exhibit hyper spectra, most do not because of variability in the spin states and low efficiency in the mixing of excited states.<sup>4</sup>

Various photochemical reactions of iron and manganese porphyrins have been documented. The photoreduction of metal porphyrin halides to  $\text{M}^{\text{II}}(\text{porph})$  and halide ion is a fairly general reaction.<sup>5</sup> In the case of  $\text{Fe}(\text{TPP})(\text{Cl})$ , photoinitiation of hydrocarbon oxidation was observed<sup>5a</sup> in the presence of  $\text{O}_2$ . In alcohol solvents,  $\text{Fe}^{\text{III}}(\text{porph})$  is photoreduced to give  $^{\bullet}\text{OR}$  and  $\text{Fe}^{\text{II}}(\text{porph})$ .<sup>6</sup> In the presence of  $\text{O}_2$  and ethanol, this reaction reduces  $\text{CCl}_4$  to  $\text{CCl}_3\text{H}$ , concomitantly oxidizing the ethanol to acetaldehyde.<sup>7</sup> The photochemical cleavage of  $[\text{Fe}(\text{TPP})]_2(\text{O})$  to  $\text{O}=\text{Fe}^{\text{IV}}(\text{TPP})$  and  $\text{Fe}^{\text{II}}(\text{TPP})$  has also been examined.<sup>8</sup> Similarly, the photoreduction of water-soluble manganese porphyrins has been reported, often with accompanying reduction of substrates upon reoxidation of the porphyrin.<sup>9</sup>

Photooxidation of the metal center is much less common. Manganese porphyrin perchlorates and periodates, for example, undergo photooxidation to a putative  $\text{O}=\text{Mn}^{\text{V}}(\text{TPP})^+$ .<sup>10</sup> This species then oxidizes a variety of organic substrates, including alkanes. In total, all four of the oxygen equivalents are used in substrate oxidation. The photoreactions of the periodate complex can be made catalytic by addition of excess soluble periodate salts. Other photooxidations of the metal center have been observed with iron<sup>11</sup> and manganese<sup>12</sup> azido complexes, each giving the metal (V) nitrido complex.

- (1) Cole, J. A.; Ferguson, S. J., Eds. *The Nitrogen and Sulphur Cycles*; Cambridge University Press: Cambridge, U.K., 1988.
- (2) Ortiz de Montellano, P. R., Ed. *Cytochrome P450*; Plenum: New York, 1985.
- (3) (a) Blauer, G.; Sund, H., Eds. *Optical Properties of Tetrapyrroles*; W. DeGruyter: Berlin, 1985. (b) Gouterman, M.; Rentzepis, P. M.; Straub, K. D., Eds. *Porphyrins: Excited States and Dynamics*; ACS Symposium Series 321; American Chemical Society: Washington, DC, 1986. (c) Andreoni, A.; Cubeddu, R., Eds. *Porphyrins in Tumor Phototherapy*; Plenum: New York, 1984. (d) Gomer, C. J. *Semin. Hematol.* **1989**, *26*, 27. (e) van der Bergh, H. *Chem. Br.* **1986**, *22*, 430.
- (4) (a) Zerner, M.; Gouterman, M. *Inorg. Chem.* **1966**, *5*, 1699. (b) Zerner, M.; Gouterman, M. *Theor. Chim. Acta* **1966**, *4*, 44. (c) Gouterman, M. In *The Porphyrins*; Dolphin, D., Ed.; Academic: New York, 1978; Vol. 3, pp 1-166.

- (5) (a) Hendrickson, D. N.; Kinnaird, M. G.; Suslick, K. S. *J. Am. Chem. Soc.* **1987**, *109*, 1243. (b) Imamura, T.; Jin, T.; Suzuki, T.; Fujimoto, M. *Chem. Lett.* **1985**, 847.
- (6) (a) Bartocci, C.; Scandola, F.; Ferri, A.; Carssiti, V. *J. Am. Chem. Soc.* **1980**, *102*, 7067. (b) Bizet, C.; Morliere, P.; Brault, D.; Delgado, O.; Bazin, M.; Suntus, R. *Photochem. Photobiol.* **1981**, *34*, 315. (c) Bartocci, C.; Amadelli, R.; Maldotti, A.; Carssiti, V. *Polyhedron* **1986**, *5*, 1297. (d) Maldotti, A.; Bartocci, C.; Locatelli, C.; Carssiti, V.; Ferri, A.; Bartolotti, F. *Inorg. Chim. Acta* **1986**, *125*, 129.
- (7) (a) Maldotti, A.; Bartocci, C.; Amadelli, R.; Carssiti, V. *J. Chem. Soc., Dalton Trans.* **1989**, 1197. (b) Bartocci, C.; Maldotti, A.; Varani, G.; Carssiti, V.; Battioni, P.; Mansuy, D. *J. Chem. Soc., Chem. Commun.* **1989**, 964.
- (8) (a) Guest, C. R.; Straub, K. D.; Hutchinson, J. A.; Rentzepis, P. M. *J. Am. Chem. Soc.* **1988**, *110*, 5276. (b) Peterson, M. W.; Rivers, D. S.; Richman, R. M. *J. Am. Chem. Soc.* **1985**, *107*, 2907. (c) Richman, R. M.; Peterson, M. W. *J. Am. Chem. Soc.* **1982**, *104*, 5795.
- (9) (a) Carnier, N.; Harriman, A. *J. Photochem.* **1981**, *15*, 341. (b) Harriman, A.; Porter, G. *J. Chem. Soc., Faraday Trans. 2* **1980**, *76*, 1429. (c) Harriman, A.; Porter, G. *J. Chem. Soc., Faraday Trans. 2* **1979**, *75*, 1543.
- (10) (a) Suslick, K. S.; Acholla, F. V.; Cook, B. R. *J. Am. Chem. Soc.* **1987**, *109*, 2812. (b) Suslick, K. S.; Acholla, F. V.; Cook, B. R.; Kinnaird, M. G. *Recl. Trav. Chim. Pays-Bas* **1987**, *106*, 329.
- (11) (a) Rehorek, D.; Berthold, T.; Hennig, H.; Kemp, T. *J. Z. Chem.* **1988**, *28*, 72. (b) Buchler, J. W.; Dreher, C. *Z. Naturforsch.* **1984**, *39B*, 222.
- (12) Groves, J. T.; Takahashi, T. *J. Am. Chem. Soc.* **1983**, *105*, 2073.

## Results and Discussion

Among the important biological functions of metalloporphyrins are the reduction of oxoanions<sup>1</sup> (such as  $\text{NO}_3^-$ ,  $\text{NO}_2^-$ ,  $\text{SO}_3^-$ , etc.) and the oxidation of hydrocarbons<sup>2</sup> (e.g., hydroxylation or epoxidation). Our results with the photochemistry of metalloporphyrin nitrate and nitrite complexes show both reaction patterns.

There are in general two types of bacterial nitrate and nitrite reductase: assimilatory and dissimilatory.<sup>13</sup> In both, prior reduction of nitrate to nitrite is necessary. Assimilatory nitrite reductase catalyzes the six-electron reduction of nitrite to ammonia, with nitrate thus serving as a nitrogen source for amino acid synthesis. Dissimilatory nitrite reductase catalyzes nitrite reduction to nitrous oxide or dinitrogen, a process known as denitrification. In this case, nitrate serves as an electron acceptor during oxidation of an organic substrate. Dissimilatory nitrite reductases usually contain two heme *cd* units at the active site, with the proposed mechanism requiring reduction of bound nitrate to nitrite, followed by conversion of nitric oxide and to then nitrous oxide or dinitrogen.<sup>14</sup> The role of nitric oxide as an intermediate in this mechanism, following some controversy, has been recently established.<sup>15</sup>

The importance of denitrification to soil nitrogen content, its application to removal of nitrogen oxide pollutants, and the challenge of understanding bacterial processes have prompted a number of investigators to model the reduction of nitrate and nitrite electrochemically and photochemically. Among the electrochemical models are coordination complexes,<sup>16</sup> modified electrodes,<sup>17</sup> cyclams,<sup>18</sup> and simple platinum electrodes.<sup>19</sup> Reduction of both nitrate and nitrite to ammonia has been accomplished photochemically with nitrate and nitrite reductases as *in vitro* enzymatic catalysts and photogenerated viologen radical as an electron carrier.<sup>20</sup> Similar photoreductions have been observed with Pt-TiO<sub>2</sub> suspensions and powders.<sup>21</sup> The reduction of nitrate to nitrite has also been accomplished with various organic sensitizers.<sup>22</sup>

Biological oxidations reveal another aspect of the diverse redox chemistry of metalloporphyrins. Because cytochrome P450 has a critical role in a wide variety of oxygenations, numerous investigations of synthetic analogues of P450 continue.<sup>23</sup> The mechanism of P450 consists of several distinct steps, the first being the binding of substrate to the Fe(III) reaction center. This is followed by a one-electron reduction of the iron center and O<sub>2</sub> binding. After a second one-electron reduction, it is proposed that an O=Fe<sup>IV</sup> porphyrin  $\pi$ -cation-radical species is formed. It is this metal-oxo species that oxidizes substrates, thereby regen-

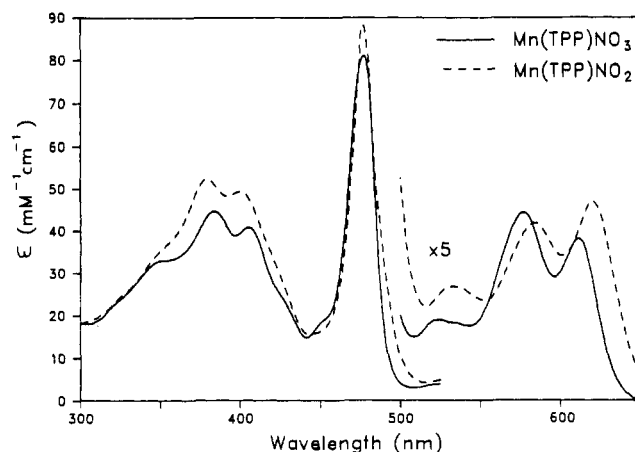


Figure 1. Electronic spectra of Mn(TPP)(NO<sub>x</sub>) complexes in benzene: (A) (—) Mn(TPP)(NO<sub>3</sub>) ( $\lambda_{\text{max}}$  = 384, 406, 478, 577, 611 nm); (B) (---) Mn(TPP)(NO<sub>2</sub>) ( $\lambda_{\text{max}}$  = 380, 400, 476, 583, 620 nm).

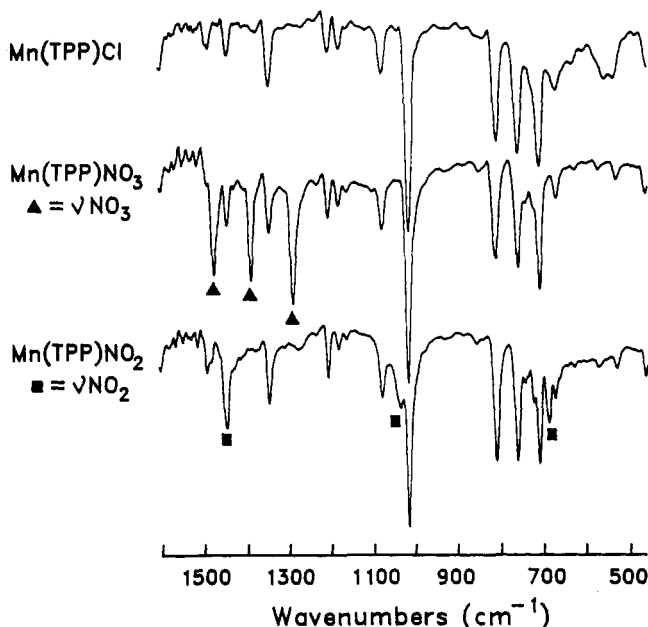


Figure 2. Infrared spectra of Mn porphyrin complexes (KBr pellet): (A) Mn(TPP)(Cl); (B) Mn(TPP)(NO<sub>3</sub>) ( $\nu(\text{NO}_3)$  = 1474, 1385, 1286 cm<sup>-1</sup>); (C) Mn(TPP)(NO<sub>2</sub>) ( $\nu(\text{NO}_2)$  = 1444, 1029, 682 cm<sup>-1</sup>).

- (13) (a) Delwiche, C. C., Ed. *Denitrification, Nitrification, and Atmospheric Nitrous Oxide*; Wiley, New York, 1981. (b) Payne, W. I. *Denitrification*; Wiley: New York, 1981.
- (14) Payne, W. I.; Riley, P. S.; Cox, C. D., Jr. *J. Bacteriol.* **1971**, *106*, 356.
- (15) Zafiriou, O. C.; Hanley, Q. S.; Snyder, G. *J. Biol. Chem.* **1989**, *264*, 5694.
- (16) (a) Rhodes, M. R.; Meyer, T. J. *Inorg. Chem.* **1988**, *27*, 4772. (b) Murphy, W. R., Jr.; Takeuchi, K.; Barley, M. H.; Meyer, T. J. *Inorg. Chem.* **1986**, *25*, 1041.
- (17) Kuwabata, S.; Uezumi, S.; Tanaka, K.; Tanaka, T. *Inorg. Chem.* **1986**, *25*, 3018.
- (18) Taniguchi, I.; Nakashima, N.; Yasakouchi, K. *J. Chem. Soc., Chem. Commun.* **1986**, 1814.
- (19) Li, H.; Robertson, D. H.; Chambers, J. Q.; Hobbs, D. T. *J. Electrochem. Soc.* **1988**, *135*, 1154.
- (20) Willner, I.; Lapidot, N.; Riklin, A. *J. Am. Chem. Soc.* **1989**, *111*, 1883.
- (21) (a) Kudo, A.; Domen, K.; Maruya, K.; Onishi, T. *Chem. Lett.* **1987**, 1019. (b) Halmann, M.; Tobin, J.; Zuckerman, K. *J. Electroanal. Chem. Interfacial Electrochem.* **1982**, *209*, 405.
- (22) Frank, A. J.; Gratzel, M. *Inorg. Chem.* **1982**, *21*, 3834.
- (23) Recent leading references: (a) Groves, J. T.; Watanabe, Y. *J. Am. Chem. Soc.* **1988**, *110*, 8443. (b) Mansuy, D.; Battioni, P. In *Activation and Functionalization of Alkanes*; Hill, C. L., Ed.; Wiley: New York, 1989; pp 195–218. (c) Suslick, K. S. *Ibid.*, pp 219–241. (d) Traylor, T. G.; Ciccone, J. P. *J. Am. Chem. Soc.* **1989**, *111*, 8413. (e) Castellino, A. J.; Bruice, T. C. *J. Am. Chem. Soc.* **1988**, *110*, 158. (f) Rodriguez, R. E.; Kelly, H. C. *Inorg. Chem.* **1989**, *28*, 589. (g) Nappa, M. J.; McKinney, R. J. *Inorg. Chem.* **1988**, *27*, 3740. (h) Battioni, P.; Renauld, J. P.; Bartoli, J. F.; Reina-Artiles, M.; Fort, M.; Mansuy, D. *J. Am. Chem. Soc.* **1988**, *110*, 8462.

erating the Fe(III) center. The discovery that the addition of exogenous oxygen atom donors could generate substrate oxidation directly (the so-called peroxide shunt),<sup>24</sup> eliminating the need for O<sub>2</sub> binding, has greatly facilitated the modeling of P450. The use of oxygen donors such as peroxyacids, hydroperoxides, iodobenzene, and oxyhalides to generate high-valent oxo species with metalloporphyrins has been established.<sup>23</sup> Through these studies, our understanding of the reactivity of high-valent oxo-metalloporphyrin complexes has developed. Although the active species of cytochrome P450 itself has yet to be directly observed, results of these model studies strongly suggest O=Fe<sup>IV</sup>(por<sup>+</sup>) as the active oxidant.

**Synthesis and Characterization.** We have successfully synthesized Mn(TPP)(NO<sub>3</sub>) and Mn(TPP)(NO<sub>2</sub>) and solved the single-crystal X-ray structure of each. Mn(TPP)(NO<sub>2</sub>) was prepared in 80% yield by the reaction of Mn(TPP)(Cl) with AgNO<sub>3</sub>(aq) in a biphasic CH<sub>2</sub>Cl<sub>2</sub>/H<sub>2</sub>O reaction mixture. The formation of insoluble AgCl effectively removes Cl<sup>-</sup> from the

- (24) (a) Rahimtula, A. D.; O'Brien, P. J. *Biochem. Biophys. Res. Commun.* **1974**, *60*, 440. (b) Lichtenberger, F.; Nastainczyk, W.; Ullrich, V. *Biochem. Biophys. Res. Commun.* **1976**, *70*, 939. (c) Hrycay, E. G.; Gustafsson, J. A.; Ingelman-Sundberg, M.; Ernster, L. *Eur. J. Biochem.* **1976**, *61*, 43.

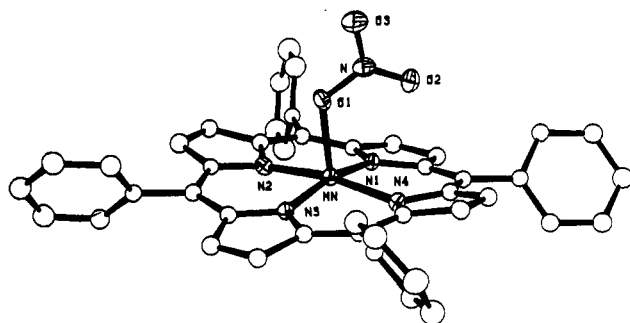


Figure 3. ORTEP diagram of  $\text{Mn}(\text{TPP})(\text{NO}_3)$  showing the atom-labeling scheme used in all tables.

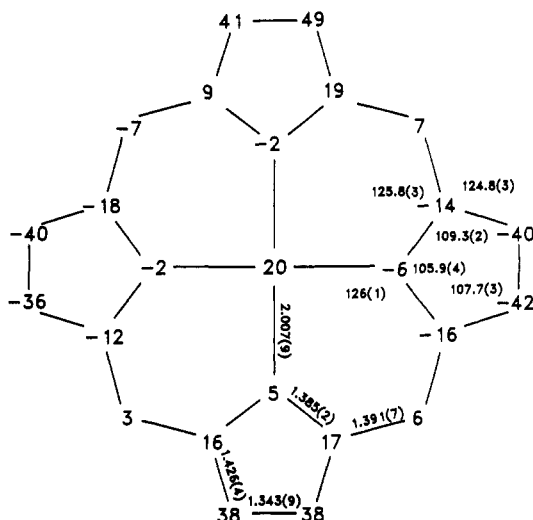


Figure 4. Formal diagram of the porphyrinato core of  $\text{Mn}(\text{TPP})(\text{NO}_3)$  with average bond distances and angles in the core and displacement of atoms from the mean 24-atom plane (in 0.01 Å units).

reaction mixture, allowing the weaker binding  $\text{NO}_3^-$  to coordinate. The product was identified by its new UV-visible spectrum (Figure 1A) and by field desorption mass spectroscopy, which shows a strong parent ion cluster at 729 amu. The infrared spectrum (Figure 2B) contains three new absorbances (vs  $\text{Mn}(\text{TPP})(\text{Cl})$ ) for nitrate coordination at 1474, 1385, and 1286  $\text{cm}^{-1}$ , consistent with monodentate coordination via a single nitrate oxygen.<sup>25</sup> Attempts at synthesizing  $\text{Mn}(\text{TPP})(\text{NO}_2)$  by the same silver salt method were unsuccessful. The compound could be made in high yield by a modification of the procedure used to synthesize  $\text{Mn}(\text{TPP})(\text{Cl})$ .<sup>26</sup> Accordingly,  $\text{H}_2\text{TPP}$  was first metalated in DMF by using  $\text{Mn}(\text{OAc})_2$ . Precipitation of the porphyrinic material by the addition of saturated aqueous  $\text{NaNO}_2$  results in replacement of the weakly coordinating acetate anion with  $\text{NO}_2^-$ . Subsequent drying and recrystallization gives the pure material in 70% yield. The infrared spectrum reveals three new bands due to the O-bound nitrite ion coordination at 1444, 1029, and 682  $\text{cm}^{-1}$  (Figure 2C). While in many cases nitrito (O-bound) complexes are not stable toward decomposition or isomerization to nitro (N-bound) coordination,<sup>27</sup> this complex is stable both in the solid and in solution for at least several weeks. The similarity of the electronic spectra (Figure 1) for  $\text{Mn}(\text{TPP})(\text{NO}_3)$  and  $\text{Mn}(\text{TPP})(\text{NO}_2)$  is not surprising, given the similarity between their primary coordination spheres.

**Crystal Structures.** Crystals of  $\text{Mn}(\text{TPP})(\text{NO}_3) \cdot 2\text{C}_6\text{H}_6$  suitable for X-ray analysis were obtained by the slow diffusion of pentane into a benzene solution. The solved structure confirms the

Table I. Crystallographic Data for  $\text{Mn}(\text{TPP})(\text{NO}_3)$  and  $\text{Mn}(\text{TPP})(\text{NO}_2)$

	$\text{Mn}(\text{TPP})(\text{NO}_3) \cdot 2\text{C}_6\text{H}_6$	$\text{Mn}(\text{TPP})(\text{NO}_2) \cdot \text{C}_6\text{H}_6$
Crystal Parameters <sup>a</sup>		
space group	triclinic $P\bar{1}$	orthorhombic $Pccn$
$a$ , Å	13.271 (4)	21.631 (11)
$b$ , Å	13.610 (5)	19.941 (12)
$c$ , Å	12.880 (3)	17.991 (6)
$\alpha$ , deg	111.44 (2)	90
$\beta$ , deg	95.71 (2)	90
$\gamma$ , deg	85.50 (3)	90
$Z$	2	8
$D_{\text{calcd}}$ , $\text{g cm}^{-3}$	1.367	1.355
cryst dims, mm	$0.3 \times 0.6 \times 0.6$	$0.4 \times 0.5 \times 0.8$
$\mu_{\text{calcd}}$ , $\text{cm}^{-1}$	3.45	3.72
$V$ , Å <sup>3</sup>	2152 (2)	7760 (7)
Data Measurement		
diffractometer	Enraf-Nonius CAD4	Enraf-Nonius CAD4
radiation	Mo $K\alpha$ (0.710 73 Å)	Mo $K\alpha$ (0.710 73 Å)
monochromator	graphite crystal ( $2\theta = 12^\circ$ )	graphite crystal ( $2\theta = 12^\circ$ )
reflcns measd	$\pm h, \pm k, -l$	$-h, +k, -l$
$2\theta$ range, deg	2.0–32.0	2.0–32.0
scan method	$\omega/\theta$	$\omega/\theta$
scan speed, deg/min	3(min), 16(max)	3(min), 16(max)
no. of rflns collected	6403	6931
no. of unique rflns	5965 ( $R_i = 0.020$ )	6052 ( $R_i = 0.030$ )
no. of obsd rflns	4890 ( $I > 2.58\sigma(I)$ )	3820 ( $I > 2.58\sigma(I)$ )
rng trnsm fctrs	0.911(max), 0.694(min)	0.891(max), 0.812(min)
$R(F)$	0.063	0.062
$R_w(F)$	0.086	0.096

<sup>a</sup> In this and all subsequent tables the esd's of all parameters are given in parentheses, right-justified to the least significant digit(s) given.

Table II. Selected Bond Lengths (Å) and Angles (deg) in  $\text{Mn}(\text{TPP})(\text{NO}_3)$

Bond Lengths			
Mn–N1	2.004 (3)	Mn–O2	3.151 (4)
Mn–N2	2.009 (3)	O1–N	1.298 (5)
Mn–N3	2.019 (3)	O2–N	1.226 (5)
Mn–N4	1.997 (3)	O3–N	1.226 (5)
Mn–O1	2.101 (3)		
Bond Angles			
N1–Mn–O1	103.9 (1)	Mn–O1–N	124.6 (3)
N2–Mn–O1	91.2 (1)	O1–N–O2	118.8 (4)
N3–Mn–O1	89.8 (1)	O1–N–O3	119.1 (4)
N4–Mn–O1	99.3 (1)	O2–N–O3	122.1 (4)

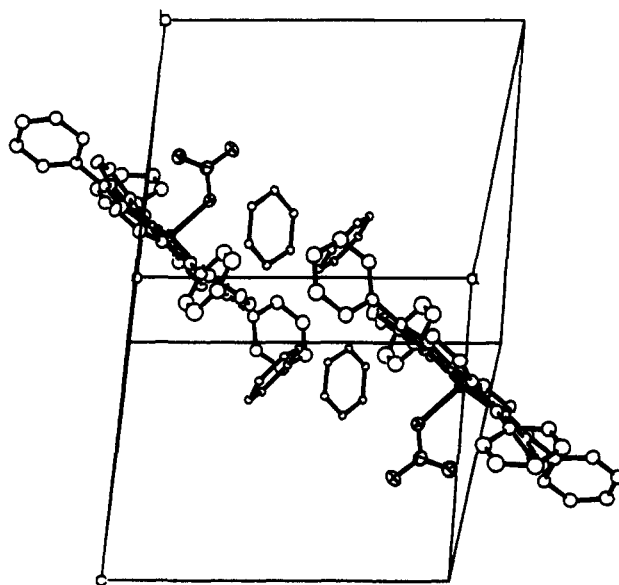


Figure 5. Unit cell packing arrangement of  $\text{Mn}(\text{TPP})(\text{NO}_3)$ .

monodentate coordination mode predicted from the IR spectrum. Figure 3 gives a view of a single molecule along with the atomic numbering scheme. Selected bond distances and angles are given

- (25) Nakamoto, K. *Infrared and Raman Spectra of Inorganic and Coordination Compounds*, 3rd ed.; Wiley: New York, 1978; pp 244–247.  
 (26) (a) Boucher, L. J. *J. Am. Chem. Soc.* **1968**, *90*, 6640. (b) Boucher, L. J. *Coord. Chem. Rev.* **1972**, *7*, 289.  
 (27) (a) Finnegan, M. G.; Lappin, A. G.; Scheidt, W. R. *Inorg. Chem.* **1990**, *29*, 181. (b) Gentile, I.; Nordin, E. *Inorg. Chem.* **1979**, *18*, 1869.

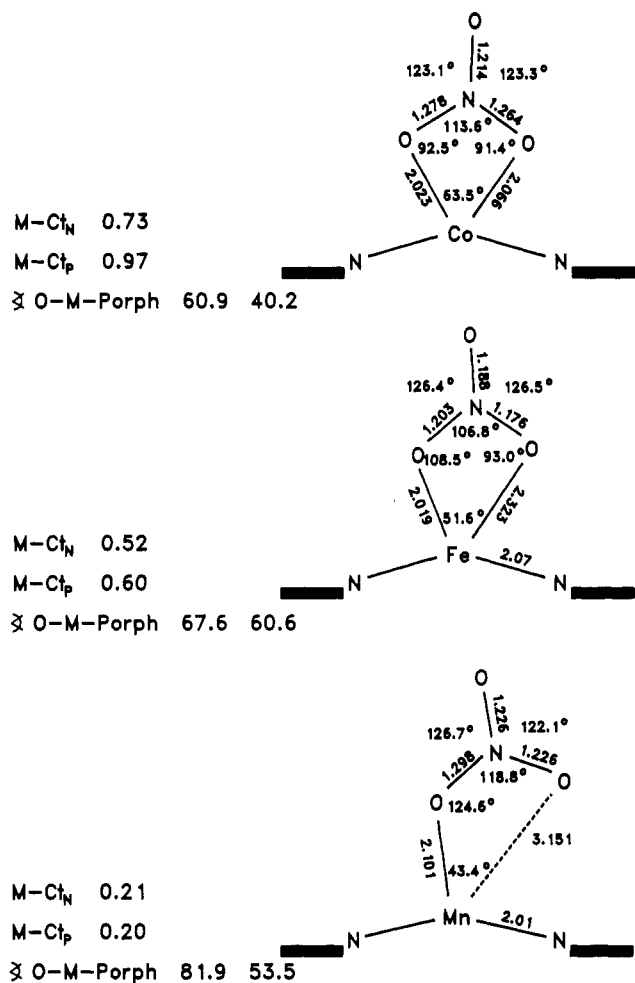


Figure 6. Comparison of the nitrate coordination to Co(porph), Fe(TPP), and Mn(TPP). The cobalt species is actually a bis-N-alkylated octaethylporphyrin species.

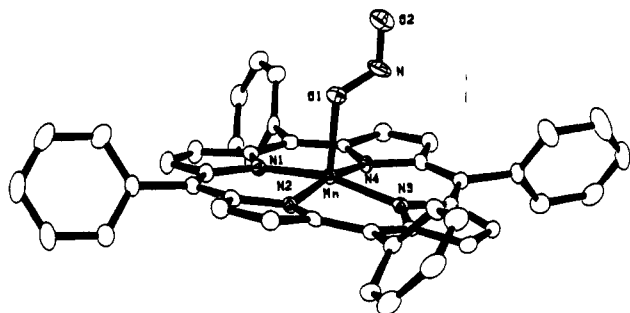


Figure 7. ORTEP diagram of Mn(TPP)(NO<sub>2</sub>) showing the atom-labeling scheme used in all tables.

in Table II. Figure 4 gives the displacements of each atom from the 24-atom core showing an  $S_4$  ruffling. Figure 5 shows the unit cell packing arrangement.

The average Mn-N<sub>por</sub> bond distance of 2.007 Å and the manganese-core displacement of 0.21 Å are consistent with values expected for Mn(III) porphyrins.<sup>28</sup> The axial Mn-O bond length of 2.101 (3) Å falls into the range seen for other manganese porphyrins with O-bound axial ligands.<sup>29</sup> The Mn-O distance, however, is slightly greater than the metal-oxygen distances reported for Co(porph)(NO<sub>3</sub>)<sup>30</sup> and Fe(TPP)(NO<sub>3</sub>),<sup>31</sup> 2.023 and

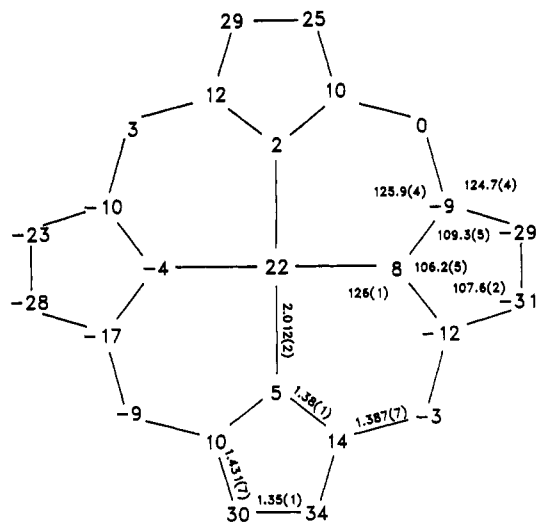


Figure 8. Formal diagram of the porphyrinato core of Mn(TPP)(NO<sub>2</sub>) with average bond distances and angles in the core and displacement of atoms from the mean 24-atom plane (in 0.01 Å units).

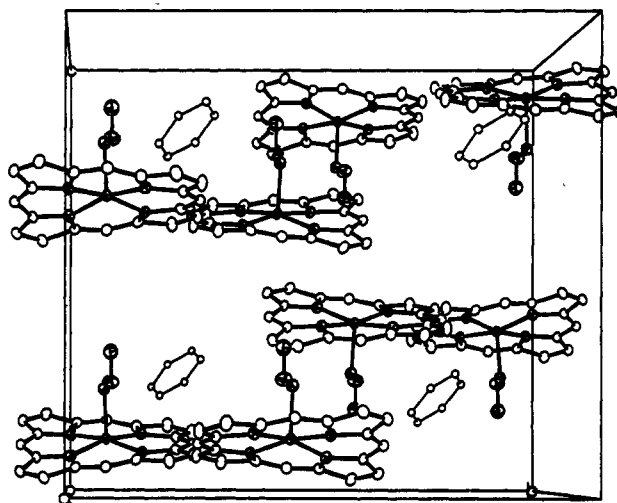


Figure 9. Unit cell packing arrangement of Mn(TPP)(NO<sub>2</sub>). The porphyrin phenyl rings and solvent disorder have been removed for clarity.

Table III. Selected Bond Lengths (Å) and Angles (deg) in Mn(TPP)(NO<sub>2</sub>)

Bond Lengths			
Mn-N1	2.012 (5)	Mn-O1	2.059 (4)
Mn-N2	2.014 (4)	O1-N	1.301 (7)
Mn-N3	2.009 (5)	O2-N	1.202 (8)
Mn-N4	2.014 (4)		
Bond Angles			
N1-Mn-O1	97.0 (2)	N4-Mn-O1	97.1 (2)
N2-Mn-O1	94.3 (2)	Mn-O1-N	115.6 (4)
N3-Mn-O1	97.6 (2)	O1-N-O2	114.8 (5)

2.019 Å, respectively. As shown in Figure 6, the nitrate coordination mode differs among these three complexes. Unlike Mn(TPP)(NO<sub>3</sub>), both the cobalt and the iron nitrates are symmetrically bidentate, almost perfectly so in the cobalt structure. Both the d<sup>5</sup> iron and the d<sup>6</sup> cobalt complexes are high-spin, which results in occupancy of the d(x<sup>2</sup> - y<sup>2</sup>) orbital. This occupancy "pushes" the metal out of the porphyrin plane to relieve the steric repulsion. While our manganese complex is also high-spin, it is only d<sup>4</sup>. This leaves the d(x<sup>2</sup> - y<sup>2</sup>) orbital unoccupied, which allows the manganese to sit further in the plane of the porphyrin. In this way, the unique monodentate coordination and longer M-O bond length of our manganese may result from the smaller metal

(28) Scheidt, W. R. In *The Porphyrins*; Dolphin, D., Ed.; Academic: New York, 1978; pp 463-512.

(29) We have also prepared and solved the structures of [Mn(TPP)]<sub>2</sub>(SO<sub>4</sub>), Mn(TPP)(OSO<sub>3</sub>H), and Mn(TPP)(ClO<sub>4</sub>), which have axial Mn-O distances of 2.005, 2.078, and 2.18 Å, respectively.

(30) Batten, P.; Hamilton, A. L.; Johnson, A. W.; Mahendran, M.; Ward, D.; King, T. J. *J. Chem. Soc., Perkin Trans. 1* 1977, 1623.

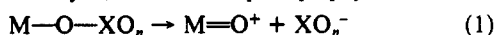
(31) Phillippi, M. A.; Baenziger, N.; Goff, H. M. *Inorg. Chem.* 1981, 20, 3904.

out-of-plane displacement: greater steric interaction between axial ligand and porphyrin ring in the manganese complex would have resulted for bidentate coordination. The remainder of the nitrate N–O bonds and angles of  $\text{Mn}(\text{TPP})(\text{NO}_3)$  are in agreement with other monodentate nitrates.<sup>32</sup>

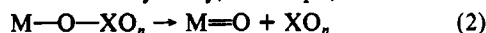
The solved X-ray structure of  $\text{Mn}(\text{TPP})(\text{NO}_2)\cdot\text{C}_6\text{H}_6$  reveals a unique monodentate O-bound coordination mode (Figure 7). As before, this is consistent with the infrared data. As in the case of the  $\text{NO}_3$  complex, the average Mn–N<sub>por</sub> bond distance of 2.012 Å and the manganese-core displacement of 0.22 Å are consistent with values expected for Mn(III) porphyrins. Figure 8 shows the  $S_4$  ruffling of the porphyrin core that was also observed in the nitrate complex and is common in manganese(III) porphyrins. Selected distances and angles are given in Table III. The placement of solvent molecules is shown in the unit cell packing diagram in Figure 9.

The coordination mode is distinctly different from that observed in the only two other porphyrin  $\text{NO}_2$  complexes known to us. Both the cobalt<sup>32</sup> and the iron<sup>33</sup> nitrite complexes are bound through the nitrogen atom of the nitrite moiety. This difference may be due largely to the lesser displacement of the Mn from the porphyrin core, resulting in greater steric repulsion for an N-bound nitrite. The manganese–oxygen bond length of 2.059 (4) Å is slightly shorter than that seen in the nitrate complex. The similarity in axial ligation of the two complexes is reflected in their electronic absorption spectra (Figure 1). Examination of the N–O bond lengths of the nitrite ion in our complex reveals a shorter N–O distance for the unligated oxygen vs the ligated oxygen (1.202 (8) Å vs 1.301 (7) Å), reflecting its expected double-bond character. The bond angles and distances of the nitrate ion itself are quite similar to those of other inorganic nitrito complexes.<sup>34</sup>

**Photochemistry.** Upon photolysis of metalloporphyrin complexes of  $\text{NO}_3^-$ ,  $\text{NO}_2^-$ ,  $\text{ClO}_4^-$ , and  $\text{IO}_4^-$ , we observe oxygen atom transfer and formation of metal–oxo species. This  $\beta$ -bond cleavage can occur either homolytically or heterolytically. If the cleavage of oxoanions is heterolytic, as shown in eq 1, a porphyrin metal–oxo



species two oxidation states above the starting material is formed. In the case of manganese and iron porphyrins, this would be a  $[\text{M}(\text{porph})(\text{O})]^+$  species, the manganese and iron forms of which are known to be competent oxidizers of hydrocarbons.<sup>35</sup> However, if the cleavage occurs homolytically, as in eq 2, the metal–oxo



species is only one oxidation state higher (e.g.,  $\text{O}=\text{M}^{\text{IV}}(\text{porph})$ ). These species are usually capable of epoxidation but are not able to oxidize C–H bonds.<sup>35</sup> While the  $\text{O}=\text{Mn}^{\text{IV}}(\text{porph})$  species is stable enough at room temperature to make direct observation possible, the  $\text{O}=\text{Fe}^{\text{IV}}(\text{porph})$  and both  $\text{O}=\text{M}(\text{porph})^+$  species react too quickly to be easily observed. Among the factors that may determine the reaction pathway are (1) the nature of the excited-state species initially formed, (2) the relative stabilities of the neutral or cationic porphyrin species formed, (3) the relative stabilities of the radical or anion leaving group, and (4) relative solvation energies of products.

Irradiation between 350 and 420 nm of  $\text{Mn}(\text{TPP})(\text{NO}_3)$  results in a clean two-step reaction process as shown in Figure 10. The conversion of  $\text{Mn}(\text{TPP})(\text{NO}_3)$  to  $\text{O}=\text{Mn}^{\text{IV}}(\text{TPP})$  takes place in the first step with a quantum yield of  $1.6 \times 10^{-4}$ . Isosbestic points occur at 622, 553, 492, 391, and 322 nm. The identification of  $\text{O}=\text{Mn}^{\text{IV}}(\text{TPP})$  is based upon its distinctive optical spectrum, upon its reactivity with a variety of substrates, and upon the overall stoichiometry and porphyrin oxidation state of the subsequent

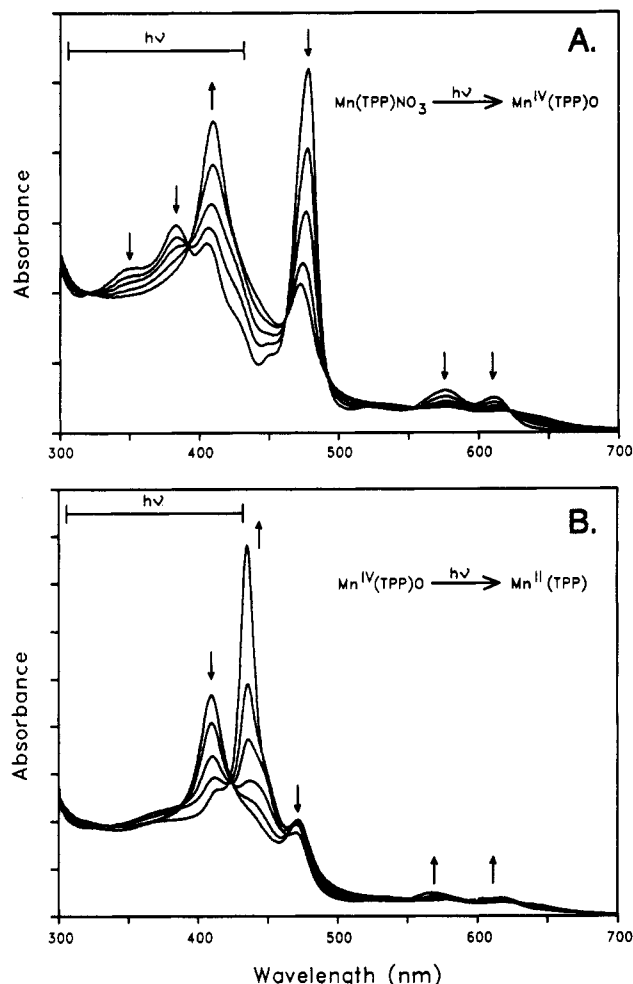
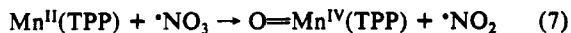
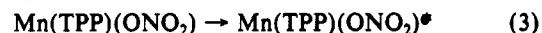


**Figure 10.** Photolytic conversion of  $\text{Mn}(\text{TPP})(\text{NO}_3)$  in benzene on irradiation from 350 to 440 nm. Arrows indicate the change in absorbance during irradiation: (A) initial production of  $\text{O}=\text{Mn}^{\text{IV}}(\text{TPP})$  with isosbestic points at 622, 553, 492, 391, and 322 nm; (B) reduction to  $\text{Mn}^{\text{II}}(\text{TPP})$  upon reaction with substrate.

reaction.<sup>36</sup> This conversion to  $\text{O}=\text{Mn}^{\text{IV}}(\text{TPP})$  does not occur upon irradiation into the Q-bands or the Soret band (i.e. > 420 nm) as determined with band-pass filters. This observation is consistent with previous manganese–porphyrin photochemical studies that showed in most cases only the bands to the blue of the Soret band (N, L, M bands) are photoactive.<sup>9,10</sup>

The formation of  $\text{O}=\text{Mn}^{\text{IV}}(\text{TPP})$  could arise from two different mechanisms. In the first, homolytic  $\beta$ -cleavage directly forms the  $\text{Mn}(\text{IV})$  complex and  $\text{NO}_2$  from the excited-state species (eq 4). Alternatively, homolytic  $\alpha$ -cleavage to produce  $\text{Mn}^{\text{II}}(\text{TPP})$  and  $\text{NO}_3$  as shown in eq 5 may be the first step. The pair may then recombine to give starting material (eq 6), to give  $\text{O}=\text{Mn}^{\text{IV}}(\text{TPP})$  and  $\text{NO}_2$  (eq 7) or to give  $\text{Mn}(\text{TPP})^+$  and  $\text{NO}_3^-$  (eq 8). In either



(32) Kaduk, J. A.; Scheidt, W. R. *Inorg. Chem.* 1974, 13, 1875.

(33) Nasri, H.; Goodwin, J. A.; Scheidt, W. R. *Inorg. Chem.* 1990, 29, 185.

(34) (a) Finney, A. J.; Hitchman, M. A.; Raston, C. L.; Rowbottom, G. L.; White, A. H. *Aust. J. Chem.* 1981, 34, 2047. (b) Wilson, R. D.; Bau, R. J. *Organomet. Chem.* 1980, 191, 123. (c) Greenwood, N. N.; Ernschaw, A. *Chemistry of the Elements*; Pergamon: Oxford, U.K., 1986; pp 531–536.

(35) Hill, C. L., Ed. *Activation and Functionalization of Alkanes*; Wiley: New York, 1989; pp 243–279.

(36) (a) Czernuszewicz, R. S.; Su, Y. O.; Stern, M. K.; Macor, K. A.; Kim, D.; Groves, J. T.; Spiro, T. G. *J. Am. Chem. Soc.* 1988, 110, 4158. (b) Groves, J. T.; Stern, M. K. *J. Am. Chem. Soc.* 1988, 110, 8628. (c) Rodgers, K. R.; Goff, H. M. *J. Am. Chem. Soc.* 1988, 110, 7049. (d) Groves, J. T.; Stern, M. K. *J. Am. Chem. Soc.* 1987, 109, 3812. (e) Schappacher, M.; Weiss, R. *Inorg. Chem.* 1987, 26, 1190.

scenario, the fate of the initial photoproducts is influenced by several factors, including their stability and that of their possible secondary products. Equation 6 could explain the low observed quantum yield of O atom transfer, since recombination would be a rapid process.

In the second step of the photoreaction,  $\text{O}=\text{Mn}^{\text{IV}}(\text{TPP})$  is converted to  $\text{Mn}^{\text{II}}(\text{TPP})$  by reaction with oxidizable substrate, as depicted in Figure 10B. The  $\text{Mn}^{\text{II}}(\text{TPP})$ , formed in >95% yield, was identified from its electronic and EPR spectra.<sup>37</sup> The reduction to  $\text{Mn}^{\text{II}}$  is accompanied by substrate oxidation (Table IV). While the oxidation of substrates by  $\text{O}=\text{Mn}^{\text{IV}}(\text{TPP})$  is known to occur thermally, irradiation accelerates the reaction severalfold. In the presence of  $\text{P}(\text{C}_6\text{H}_5)_3$ , 2.0 equiv of  $\text{OP}(\text{C}_6\text{H}_5)_3/\text{equiv}$  of  $\text{Mn}(\text{TPP})(\text{NO}_3)$  is formed during the second step. Due to the facile oxidation of the phosphine, we take this to be the maximum number of oxidation equivalents available from  $\text{Mn}(\text{TPP})(\text{NO}_3)$ . With alkenes as substrates, epoxidation is observed, although in lower yield. Styrene results in a little more than 1 equiv of oxidation product/equiv of  $\text{Mn}(\text{TPP})(\text{NO}_3)$ , or roughly 52% of the maximum yield. This is comparable to yields observed in thermal epoxidations.<sup>23</sup> As expected for  $\text{O}=\text{Mn}^{\text{IV}}(\text{TPP})$ , no hydroxylation of C—H bonds was observed, even with activated sites (e.g., benzylic bonds in toluene).

To identify the source of the second oxidizing equivalent, we synthesized separately the presumed intermediate,  $\text{Mn}(\text{TPP})(\text{NO}_2)$ . This compound shows identical transformations as  $\text{Mn}(\text{TPP})(\text{NO}_3)$  upon irradiation into the N, L, and M bands to the blue of the Soret band. With the nitrite complex, the formation of  $\text{O}=\text{Mn}^{\text{IV}}(\text{TPP})$  occurs with a quantum yield of  $5.3 \times 10^{-4}$ , three times that seen with the nitrate complex. Reaction with  $\text{P}(\text{C}_6\text{H}_5)_3$  confirms that 1.0 equiv of  $\text{OP}(\text{C}_6\text{H}_5)_3$  is formed on reduction to  $\text{Mn}^{\text{II}}(\text{TPP})$ . The  $\text{Mn}^{\text{II}}(\text{TPP})$  species is generated in >95% yield, presumably along with 1 equiv of NO. It is likely that  $\text{Mn}(\text{TPP})(\text{NO}_2)$  is formed during the photolysis of  $\text{Mn}(\text{TPP})(\text{NO}_3)$  and may account for the small deviations from isosbestic behavior in the second phase of the reaction (Figure 10B). This proposal is reinforced by our observation that  $\text{NO}_2(\text{g})$  reacts with  $\text{Mn}^{\text{II}}(\text{TPP})$  at low concentrations to give  $\text{Mn}(\text{TPP})(\text{NO}_2)$ . Scheme I accounts for the observed reactivity and yields of substrate oxidation.

While this reaction scheme suggests that the reaction should be catalytic in the presence of excess  $\text{NO}_2$ , this proves to be experimentally difficult for two reasons. First, at higher concentrations more NO is produced, which leads to the observed formation of  $\text{Mn}(\text{TPP})(\text{NO})$ . This known compound is photostable in our hands<sup>38</sup> and therefore terminates the catalytic chain. Second, it is known<sup>39</sup> that  $\text{NO}_2$  is also photoactive at the wavelengths in question, and at higher concentrations its photochemistry would compete with that of the porphyrinic systems.

$\text{Fe}(\text{TPP})(\text{NO}_3)$  is also photoactive upon irradiation in the 350–450-nm region. The final porphyrin product observed after irradiation depends on the method of purification and reaction solution preparation. Under rigorously oxygen-free conditions,  $\text{Fe}^{\text{II}}(\text{TPP})$  is observed, and in the presence of  $\text{P}(\text{C}_6\text{H}_5)_3$ , the known species  $\text{Fe}^{\text{II}}(\text{TPP})(\text{P}(\text{C}_6\text{H}_5)_3)$  is formed.<sup>52</sup> In other cases the final product is  $[\text{Fe}(\text{TPP})]_2(\text{O})$  due to trace oxygen contamination as shown in Figure 11.  $[\text{Fe}(\text{TPP})]_2(\text{O})$  is formed quantitatively with isosbestic points at 322, 403, 431, 489, 549, and 628 nm. The quantum yield of  $\text{Fe}(\text{TPP})(\text{NO}_3)$  bleaching is  $1.26 \times 10^{-4}$ , with the  $\mu$ -oxo dimer being photostable under our reaction conditions and time scale.

Scheme I. Photochemical Reaction Cycle of Manganese Porphyrin Nitrate and Nitrite Complexes

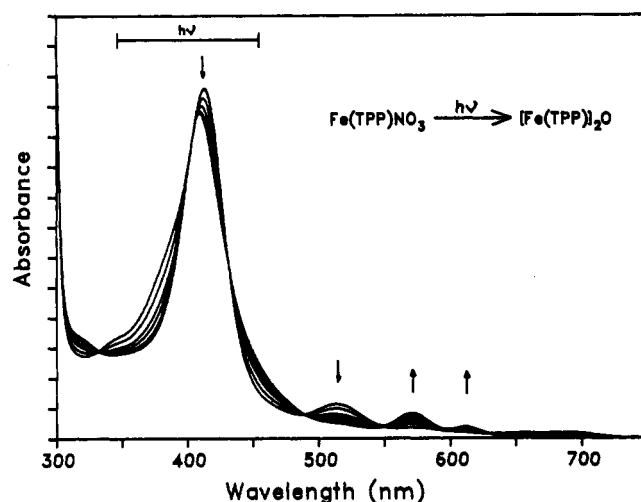
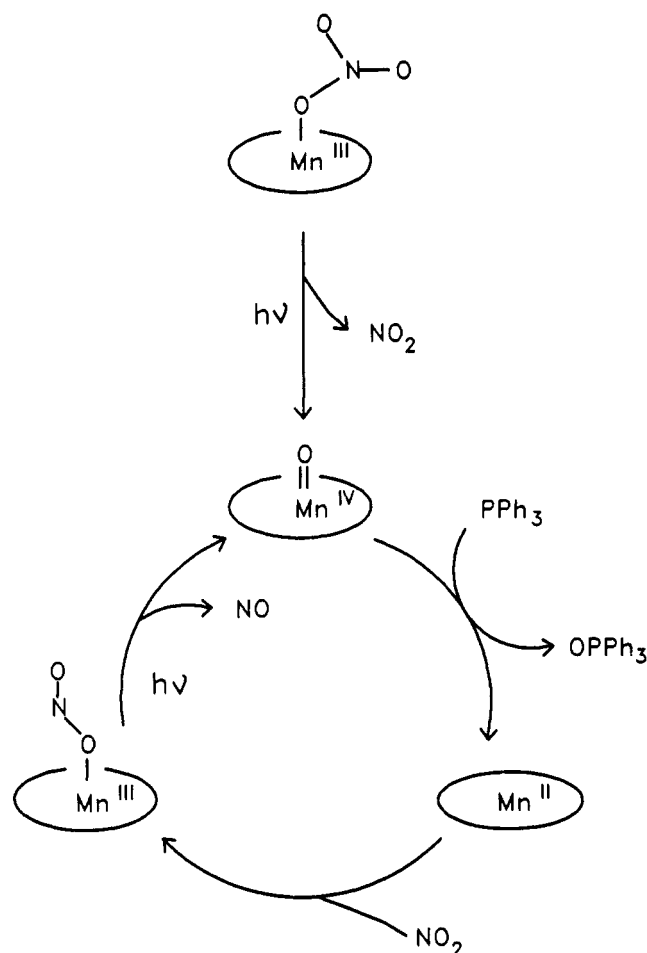
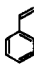
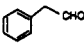
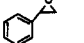
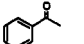
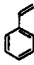
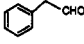
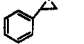
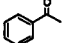
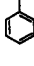
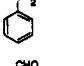



Figure 11. Photolytic conversion of  $\text{Fe}(\text{TPP})(\text{NO}_3)$  to  $[\text{Fe}(\text{TPP})]_2(\text{O})$  in benzene on irradiation into the Soret band. Arrows indicate the change in absorbance during irradiation. Isosbestic points occur at 322, 403, 431, 489, 549, and 628 nm.

- (37) (a) Reed, C. A.; Kouba, J. K.; Grimes, C. J.; Cheung, S. K. *J. Am. Chem. Soc.* **1978**, *100*, 3. (b) Hoffman, B. M.; Weschler, C. J.; Basolo, F. *J. Am. Chem. Soc.* **1976**, *98*, 5473.
- (38) On a nanosecond time scale,  $\text{Mn}(\text{TPP})(\text{NO})$  and  $\text{Fe}(\text{TPP})(\text{NO})$  are photoactive, producing  $\text{M}^{\text{II}}(\text{TPP})$  and NO, which then rapidly recombine. This would appear as photostability on the time scale of our experiments: Hoshino, M.; Kogure, M. *J. Phys. Chem.* **1989**, *93*, 5478.
- (39) (a) Pitts, J. N., Jr.; Sharp, J. H.; Chan, S. I. *J. Chem. Phys.* **1964**, *24*, 3655. (b) Blacet, F. E.; Hall, T. C.; Leighton, P. A. *J. Am. Chem. Soc.* **1962**, *84*, 4011.

Remarkable substrate oxidation occurs during these photolyses. In the presence of  $\text{P}(\text{C}_6\text{H}_5)_3$ , 2.98 equiv of  $\text{OP}(\text{C}_6\text{H}_5)_3$  is formed, indicating that all three of the nitrate oxygen atoms of  $\text{Fe}(\text{TPP})(\text{NO}_3)$  are available (Table IV). In the presence of styrene,  $2.99 \pm 0.05$  oxidizing equiv is again realized. With toluene as substrate,  $1.70 \pm 0.02$  oxidizing equiv is detected (benzaldehyde is 2 oxidizing equiv above toluene). These results taken together indicate that at least one of the oxidizing equivalents is in the form of  $\text{O}=\text{Fe}^{\text{IV}}(\text{TPP}^{++})$ ,<sup>40</sup> since  $\text{O}=\text{Fe}^{\text{IV}}(\text{TPP})$  is not capable of the

**Table IV.** Oxidation of Substrates by Mn(TPP)(NO<sub>2</sub>) and Fe(TPP)(NO<sub>3</sub>)

Porphyrin	Substrate	Product(s)	Yield/Metal *
Mn(TPP)(NO <sub>3</sub> )	PPh <sub>3</sub>	OPPh <sub>3</sub>	2.03(10)
Mn(TPP)(NO <sub>3</sub> )			0.00(3)
			0.43(7)
			0.82(8)
Mn(TPP)(NO <sub>2</sub> )	PPh <sub>3</sub>	OPPh <sub>3</sub>	1.00(12)
Fe(TPP)(NO <sub>3</sub> )	PPh <sub>3</sub>	OPPh <sub>3</sub>	2.98(7)
Fe(TPP)(NO <sub>3</sub> )			0.69(7)
			0.44(5)
			1.86(6)
Fe(TPP)(NO <sub>3</sub> )			0.06(1)
			0.82(2)

\* Yields and errors are based on determinations from at least four separate experiments for each substrate.

observed hydroxylation.<sup>41</sup> Similarly, none of the NO<sub>2</sub> species in either ground or excited states (at these wavelengths) are capable of hydroxylation. Thus, in contrast to Mn(TPP)(NO<sub>3</sub>), which undergoes homolytic bond cleavage as per eq 1, Fe(TPP)(NO<sub>3</sub>) yields the more potent oxidizer via heterolytic cleavage (eq 2). The reason for this difference in reactivity is not known.

The ultimate fate of the nitrogen in the iron system remains unknown. The combined complexity of the interreaction of the various nitrogen oxides<sup>42</sup> with the instability of iron porphyrin nitrite complexes<sup>33</sup> precludes a full analysis of the reaction pathway. Regardless, all three oxygen atoms of NO<sub>3</sub><sup>-</sup> can be made available for photochemical oxidation of substrate.

### Conclusions

The new compounds Mn(TPP)(NO<sub>3</sub>) and Mn(TPP)(NO<sub>2</sub>) have been synthesized, and their single-crystal X-ray structures have been solved. Unlike the analogous iron complex, Mn(TPP)(NO<sub>2</sub>) is very stable toward decomposition and rearrangement of the nitrite ion. In both Mn(TPP)(NO<sub>3</sub>) and Mn(TPP)(NO<sub>2</sub>), the axial ligand is monodentate, bound through an oxygen. We have shown that Mn(TPP)(NO<sub>3</sub>) can be photochemically converted via a homolytic bond cleavage to O=Mn<sup>IV</sup>(TPP) and that this species reacts to give 2 equiv of oxidized substrate and 1 equiv of Mn<sup>II</sup>(TPP). In addition, we have shown that Mn(TPP)(NO<sub>2</sub>) is photoactive and also produces O=Mn<sup>IV</sup>(TPP) on irradiation. Mn(TPP)(NO<sub>2</sub>) is the probable in-

termediate in the photolysis of Mn(TPP)(NO<sub>3</sub>), responsible for the second oxidizing equivalent. In contrast, Fe(TPP)(NO<sub>3</sub>) was shown to undergo a heterolytic bond cleavage to produce a more reactive oxidant, presumably O=Fe<sup>IV</sup>(TPP<sup>+</sup>). In this case, all three nitrate oxygens may be used in oxidation of substrates.

The reduction of nitrate and nitrite by these complexes bears striking resemblance to dissimilatory nitrate and nitrite reductases.<sup>13</sup> The conversion of NO<sub>3</sub><sup>-</sup> to NO<sub>2</sub><sup>-</sup> and then to NO by our Mn porphyrin complexes is similar to the initial steps of bacterial denitrification. In bacterial systems such as *Thiobacillus denitrificans*, the same initial steps are observed<sup>1</sup> but are followed by further reduction of NO to N<sub>2</sub>O and then to N<sub>2</sub>. These final steps may be occurring during the photolysis of Fe(TPP)(NO<sub>3</sub>) and would account for the availability of all three nitrate oxygen atoms for substrate oxidation.

In addition, the high-valent metal-oxo species formed during the oxoanion reductions are viable models for the active species in many biological systems such as P450<sup>2</sup> and the peroxidases.<sup>43</sup> The O=Mn<sup>IV</sup>(TPP) species formed by Mn(TPP)(NO<sub>3</sub>) and Mn(TPP)(NO<sub>2</sub>) is similar to compound II of peroxidase. The more reactive O=Fe<sup>IV</sup>(TPP<sup>+</sup>) presumably formed during the photolysis of Fe(TPP)(NO<sub>3</sub>) is similar to compound I of peroxidase and the postulated active species of P450.

### Experimental Section

**Materials.** Solvents used were of reagent grade and were distilled prior to use. Dichloromethane was distilled from calcium hydride, toluene was distilled from sodium, and pentane and benzene were distilled from sodium/benzophenone. Oxidation substrates (toluene, styrene, P(C<sub>6</sub>H<sub>5</sub>)<sub>3</sub>) were purchased from Aldrich Chemical Co. and purified by standard procedures.<sup>44</sup> All substrates were passed down a short column of activity I neutral alumina just prior to use to remove trace oxide contaminants and, in the case of styrene, to remove inhibitor. Purity was verified by gas chromatography. Inorganic salts were purchased from Aldrich and used without further purification. H<sub>2</sub>TPP, Mn(TPP)(Cl), and Fe(TPP)(Cl) were prepared by published methods.<sup>26,45,46</sup> Fe(TPP)(NO<sub>3</sub>), Mn(TPP)(NO), and Fe(TPP)(NO) were also synthesized by published methods.<sup>47-49</sup>

**Synthesis of Mn(TPP)(NO<sub>3</sub>).** Mn(TPP)(Cl) (200 mg, 0.28 mmol) was dissolved in 50 mL of CH<sub>2</sub>Cl<sub>2</sub>. An equal volume of saturated AgNO<sub>3</sub>(aq) was then added, and the biphasic mixture was stirred vigorously overnight. The organic layer was filtered to remove silver salts and then evaporated to dryness. The crude solid was recrystallized twice from toluene/pentane to give the purple crystals in 80% yield. Anal. Found (calcd) for Mn(TPP)(NO<sub>3</sub>): C, 72.35 (72.43); H, 3.88 (3.87); N, 9.51 (9.60); Mn, 7.51 (7.53). UV-vis in benzene at 25 °C, with wavelengths in nm (ε in L mol<sup>-1</sup> cm<sup>-1</sup>): 384 (4.4 × 10<sup>4</sup>), 406 (4.1 × 10<sup>4</sup>), 478 (8.1 × 10<sup>4</sup>), 577 (8.7 × 10<sup>3</sup>), 611 (7.4 × 10<sup>3</sup>). IR bands due to coordinated NO<sub>3</sub> (KBr pellet): 1474, 1385, 1286 cm<sup>-1</sup>.

**Synthesis of Mn(TPP)(NO<sub>2</sub>).** H<sub>2</sub>TPP (250 mg, 0.41 mmol) was dissolved in 30 mL of dimethylformamide (DMF), and the solution was heated to near reflux. Mn(OAc)<sub>2</sub> (250 mg, 1.44 mmol) was then added, and the solution was refluxed until the UV-vis spectrum showed no metal-free porphyrin remaining (about 30 min). The reaction solution was then cooled and poured into 50 mL of saturated NaNO<sub>2</sub>(aq) to precipitate the crude product. After collection by filtration, the crude solid was washed with copious water and dissolved in benzene, and the solution was dried over anhydrous NaNO<sub>2</sub>. Pentane was then added to precipitate the product. After a second recrystallization from benzene/pentane, the pure dark purple material was isolated in 70% yield. Anal. Found (calcd) for Mn(TPP)(NO<sub>2</sub>)-C<sub>6</sub>H<sub>6</sub>: C, 75.77 (75.84); H, 4.66 (4.33); N, 8.72 (8.84). UV-vis in benzene at 25 °C, with wavelengths

- (40) (a) Chin, D.; LaMar, G. N.; Balch, A. L. *J. Am. Chem. Soc.* **1980**, *102*, 5945. (b) Groves, J. T.; Quinn, R.; McMurray, T. J.; Nakamura, M.; Lang, G.; Boso, B. *J. Am. Chem. Soc.* **1985**, *107*, 354. (c) Chin, D.; LaMar, G. N.; Balch, A. L. *J. Am. Chem. Soc.* **1980**, *102*, 4344. (d) Balch, A. L.; Chan, Y. W.; Cheng, R. J.; LaMar, G. N.; Grazynski, L. L.; Renner, M. W. *J. Am. Chem. Soc.* **1984**, *106*, 7779.
- (41) (a) Labeque, R.; Marnett, L. J. *J. Am. Chem. Soc.* **1989**, *111*, 6621. (b) Groves, J. T.; Nemo, T. E. *J. Am. Chem. Soc.* **1983**, *105*, 6243. (c) Groves, J. T.; Nemo, T. E. *J. Am. Chem. Soc.* **1983**, *105*, 5786. (d) Groves, J. T.; Watanabe, Y. *J. Am. Chem. Soc.* **1986**, *108*, 507. (e) Bruce, T. C.; Ostovic, D. *J. Am. Chem. Soc.* **1989**, *111*, 6511.
- (42) Greenwood, N. N.; Earnshaw, A. *Chemistry of the Elements*; Pergamon: Oxford, U.K., 1986; pp 508-527.
- (43) Hewson, W. D.; Hager, L. P. In *The Porphyrins*; Dolphin, D., Ed.; Academic: New York, 1978; pp 295-332.
- (44) Perrin, D. D.; Armarego, W. L. F. *Purification of Laboratory Chemicals*, 3rd ed.; Pergamon: Oxford, U.K., 1988.
- (45) Adler, A. D.; Longo, F. R.; Finarelli, J. D. *J. Org. Chem.* **1967**, *32*, 476.
- (46) Fleischer, E. B.; Palmer, J. M.; Srivastava, T. S.; Chatterjee, A. *J. Am. Chem. Soc.* **1971**, *93*, 3162.
- (47) Phillippi, M. A.; Baenziger, N.; Goff, H. M. *Inorg. Chem.* **1981**, *20*, 3904.
- (48) Wayland, B. B.; Olson, L. W.; Siddiqui, Z. O. *J. Am. Chem. Soc.* **1976**, *98*, 94.
- (49) (a) Scheidt, W. R.; Frisser, M. E. *J. Am. Chem. Soc.* **1975**, *97*, 17. (b) Wayland, B. B.; Olson, L. W. *J. Chem. Soc., Chem. Commun.* **1973**, 897.



in nm ( $\epsilon$  in L mol<sup>-1</sup> cm<sup>-1</sup>): 380 ( $5.2 \times 10^4$ ), 400 ( $4.9 \times 10^4$ ), 476 ( $8.8 \times 10^4$ ), 583 ( $7.9 \times 10^3$ ), 620 ( $9.1 \times 10^3$ ). IR bands due to NO<sub>2</sub> coordination (KBr pellet): 1444, 1029, 682 cm<sup>-1</sup>.

**Instrumentation.** UV-visible spectra were recorded on either an IBM 9430 or a Hewlett-Packard 8452A diode array spectrophotometer. Infrared spectra were recorded as KBr pellets with either a Perkin-Elmer 1600 or 1750 FT-IR instrument. EPR spectra were obtained with a Bruker ESP 300 ESR X-band spectrometer operating at 9.42 GHz. Temperature was maintained by a Varian ER 4111 temperature controller. Oxidation products were analyzed on a Varian 3700 GC with a Shimadzu C-R3A integrator. P(C<sub>6</sub>H<sub>5</sub>)<sub>3</sub> and its products were analyzed with a 0.2 mm i.d., cross-linked dimethylsilicone (HP-1) column, 12.5 m long; toluene and styrene were analyzed with a similar column, 30 m long. Dodecane was used as the internal standard for calculating yields. Product identification by GC-mass spectral analysis. Elemental analyses were performed by the UIUC Microanalysis Laboratory.

**Photochemical Reactions.** All photochemical reaction solutions were prepared in a Vac-Atmospheres inert-atmosphere box (<2 ppm of O<sub>2</sub>) and sealed in cuvettes to avoid oxygen. Reaction solutions were generally 300 mM in substrate and 0.3 mM in porphyrin. All reactions were run in benzene. An aliquot of dodecane was included in each mixture as an internal standard for calculating yields from the GC trace. Yields and errors are based on determinations from at least four separate experiments for each substrate. Irradiation was carried out with a 300-W xenon arc lamp focused onto the reaction cuvette. Wavelengths were selected by the use of various band-pass filters. Cuvettes were thermostated with a water jacket. Quantum yields were determined by chemical actinometry<sup>50</sup> with Aberchrome 540. For quantum yields, the irradiation was carried out with a 450-W medium-pressure Hg-arc immersion lamp. Chemical filters were used to select only the 366-nm line.

**Structure Determination and Refinement of Mn(TPP)(NO<sub>3</sub>)-2C<sub>6</sub>H<sub>6</sub>.** Details of crystal data and intensity collection are given in Table I. The dark purple crystal used for structure determination was mounted with oil (Paratone-N, Exxon) on a thin glass fiber. The crystal had well-developed faces with no crystallites or other contaminating substances observed on the surface. The structure was solved by Patterson methods; the correct position for the manganese was deduced from a Patterson map. A weighted difference Fourier synthesis revealed positions for the atoms of the porphyrin ring, and subsequent least-squares difference Fourier calculations gave positions for the remaining non-hydrogen atoms. Hydrogen atoms were included as fixed contributors in idealized positions. In the final cycle of least squares, isotropic thermal coefficients were refined for the phenyl and benzene carbon atoms, anisotropic thermal coefficients for the remaining non-hydrogen atoms, and group isotropic thermal parameters for the porphyrin and benzene hydrogen atoms. In the final eight cycles of block-diagonal least-squares refinement, the porphyrin was refined in four cycles and the solvate molecules were refined in the last four cycles. Successful convergence was indicated by the maximum shift/error for the last cycles. The final difference Fourier map had no significant features. A final analysis of variance

between observed and calculated structure factors showed no apparent systematic errors.

**Structure Determination and Refinement of Mn(TPP)(NO<sub>2</sub>)-C<sub>6</sub>H<sub>6</sub>.** Details of crystal data and intensity collection are given in Table I. The crystal was mounted to a thin glass fiber as above. Pseudorotation photographs revealed that the crystal used for structure determination was slightly twinned, which, owing to the large crystal volume, caused occasional peak overlap. Despite this problem, the final analysis of variance showed less than 140 of 3820 observed intensities had  $\Delta/\sigma$  greater than 2. No other problems were encountered in collecting the data, and there was no change in the appearance of the sample during the experiment.

The structure was solved by direct methods (SHELX-86);<sup>51</sup> correct positions for the porphyrin non-hydrogen atoms were detected from an *E* map. Subsequent least-squares-difference Fourier calculations revealed atomic positions distinctly separate from the porphyrin. These peaks have been interpreted as disordered benzene solvate molecules. Porphyrin hydrogen atoms were included as fixed contributors in idealized positions. Positions for the disordered benzene ring carbon atoms were constrained to idealized geometry. One group (C45-C50) was disordered about the 2-fold symmetry axis along ( $1/4, 3/4, z$ ) and the second group was disordered in three positions about the 2-fold axis along ( $1/4, 1/4, z$ ). Variable site occupancies for the latter were normalized and converged to 0.15 (2), 0.26 (2), and 0.09 (2) for rings C51-C56 "A", "B", "C", respectively. The least-squares matrix was blocked to isolate atoms coordinated to the manganese, the porphyrin phenyl rings, and the disordered benzene solvate molecules. In the final cycles of the least-squares refinement, benzene ring atoms were refined as rigid groups, group isotropic thermal parameters were varied for the disordered solvate molecules, a group isotropic thermal parameter was varied for the hydrogen atoms, and anisotropic thermal coefficients were refined for the remaining non-hydrogen atoms. The highest peaks in the final differences Fourier maps were located in the vicinity of the disordered benzene rings. A final analysis of variance between observed and calculated structure factors showed a slight inverse dependence on  $\sin \theta$ .

**Acknowledgment.** This work was supported by the National Institutes of Health. We thank Dr. Scott R. Wilson and Charlotte L. Stern of the University of Illinois X-ray Crystallographic Laboratory for performing the structural analyses and Professor Gregory S. Girolami for helpful discussions. We gratefully acknowledge receipt of an NIH Research Career Development Award (K.S.S.) and an NIH Traineeship (R.A.W.).

**Supplementary Material Available:** Tables of atomic coordinates, thermal parameters, and complete bond distances and angles for Mn(TPP)(NO<sub>3</sub>) and Mn(TPP)(NO<sub>2</sub>) (15 pages); tables of final observed and calculated structure factors for Mn(TPP)(NO<sub>3</sub>) and Mn(TPP)(NO<sub>2</sub>) (37 pages). Ordering information is given on any current masthead page.

(50) (a) Heller, H. G.; Langan, J. R. *J. Chem. Soc., Perkin Trans. 2* **1981**, 341. (b) Darcy, P. J.; Heller, H. G.; Strydom, P. J.; Whittall, J. J. *Chem. Soc., Perkin Trans. 2* **1981**, 202.

(51) Sheldrick, G. M. In *Crystallographic Computing B*; Sheldrick, G. M., Kruger, G., Goddard, R., Eds.; Oxford University Press: Oxford, U.K., 1985; pp 175-189.

(52) Richman, R. M.; Peterson, M. W. *J. Am. Chem. Soc.* **1982**, *104*, 5795.